

## Design of piezoelectric transducer arrays for passive and active modal control of thin plates

Georg Zenz<sup>1</sup>, Wolfgang Berger<sup>1</sup>, Johannes Gerstmayr<sup>1</sup>, Manfred Nader<sup>1</sup> and Michael Krommer<sup>\*2</sup>

<sup>1</sup>Linz Center of Mechatronics (LCM), Altenbergerstr.69, A-4040 Linz, Austria

<sup>2</sup>Institute of Technical Mechanics, Johannes Kepler University Linz, Altenbergerstr.69, A-4040 Linz, Austria

(Received January 15, 2013, Revised May 21, 2013, Accepted July 5, 2013)

**Abstract.** To suppress vibration and noise of mechanical structures piezoelectric ceramics play an increasing role as effective, simple and light-weighted damping devices as they are suitable for sensing and actuating. Out of the various piezoelectric damping methods this paper compares mode based active control strategies to passive shunt damping for thin plates. Therefore, a new approach for the optimal placement of the piezoelectric sensors/actuators, or more general transducers, is proposed after intense theoretical investigations based on the Kirchhoff kinematical hypotheses of plates; in particular, modal and nilpotent transducers are discussed in detail. Based on the proposed distribution a discrete design for modal transducers is implemented, tested and verified on an experimental setup. For active control the modal sensors clearly identify the eigenmodes, whereas the modal actuators impose distributed eigenstrains in order to reduce the transverse plate vibrations. In contrast to the modal control, passive shunt damping works without requiring additional actuators or auxiliary power and can therefore act as an autonomous system, but it is less effective compensating the flexible vibrations. Exemplarily, an acryl glass plate disturbed by an arbitrary force initialized by a loudspeaker is investigated. Comparing the different methods their specific advantages are highlighted and a significant broadband reduction of the vibrations of up to -20dB is obtained.

**Keywords:** smart structures; plate vibrations; piezoelectric transducers; modal transducers; nilpotent transducer; shunt damping, modal control

### 1. Introduction

Smart structure technology is a key technology for the design of so-called intelligent, civil, mechanical and aerospace structures. These intelligent or smart structures automatically react to external disturbances similar to human beings. For reviews see Crawley (1994) or Tani *et al.* (1998) and future challenges and opportunities were discussed in Liu *et al.* (2005). Typically smart structures are used to meet the increasing demand for effective damping mechanisms in order to avoid undesired oscillations, structural borne sound and material fatigue, see Nader (2008). Concerning the application of smart structures for active vibration control we refer to Alkhatib and

---

\*Corresponding author, Associate Professor, E-mail: [michael.krommer@jku.at](mailto:michael.krommer@jku.at)

Golnaraghi (2003) and for noise reduction see e.g., Nestorovic *et al.* (2007). Practical applications range from wind turbines, to helicopter blades, to robot arms, to flexible space structures, and so on. Different strategies are available to reduce vibrations and have been extensively studied in the literature; e.g., active vibration control in Fuller *et al.* (1996), Preumont (2002), or shape control, which can completely compensate the oscillations by a transient distribution of actuation stresses for a known set of forces. Implementations of shape control can be found in Nader (2008), Zehetner and Irschik (2005), Irschik *et al.* (1999, 2003), Yu *et al.* (2009) for beams and in Gattringer *et al.* (2003), Nader *et al.* (2003), Krommer and Varadan (2005), Tzou *et al.* (1994) for plates and shells; for a review of shape control see Irschik (2002). A prominent example for putting smart structures into practice are piezoelectric transducers, which play an increasing role as sensors and actuators of a damping system due to their light weight, good operating characteristic and simple implementation on general components; see e.g., Hagood and von Flotow (1991), Moheimani and Fleming (2006), Niederberger (2005).

The study of smart structures requires a multi-disciplinary approach, which involves coupled multi-field modeling of the structure, the communication between the structure and a controller (enabled by means of suitable sensor and actuator systems), the structural integration of the smart system, its practical implementation and experimental verification. A key aspect within these topics is the proper functioning of the communication between the structure and the controller; this communication has been denoted as control-structure interaction in the literature, see Gabbert and Tzou (2000). In particular, sensors are responsible for converting mechanical energy into information about the state of the structure, which must be interpreted and properly processed by the controller to provide the actuator with information about what to do. A crucial point is the spatial distribution of sensors and actuators, both for monitoring as well as control, as the structures under consideration are typically continuous structures.

In the present paper the topic of optimal distribution of sensors/actuators or more general transducers in order to put distributed transducers into practice is crucial. Recently, Gupta *et al.* (2010) have reported on the various optimization criteria that are known in the literature (in particular, maximizing modal forces/moments applied by piezoelectric actuators, maximizing deflection of the host structure, minimizing control effort/maximizing energy dissipated, maximizing degree of controllability, maximizing degree of observability, and minimizing spill-over effects) and included an exhaustive list of references, to which we would like to refer the reader of the present paper. In contrast to the methods reported by Gupta *et al.* (2010), research on continuously distributed strain transducers has also attracted a lot of attention in the literature. In the framework of strain sensors (actuators can be treated analogous, if they are collocated to the sensors) the latter are also known under the notion of a spatial filter as they filter certain spatial information; e.g., the celebrated concept of modal filters, which filter the modal content of only one vibration mode of a structure (Lee and Moon 1990), displacement filters, which filter the displacement of a specific point in a specific direction (Krommer and Irschik 2007) or volume displacement filters (Preumont *et al.* 2005). Spatial filters are widely used in structural control (e.g., Preumont *et al.* 2003) and structural health monitoring (e.g., Deraemaeker and Preumont 2006). It has been mentioned in the literature that spatial filters can be put into practice either by continuously distributed sensors or approximated by arrays of dense sensors. For both cases the use of piezoelectric sensors is popular; on the one hand, because piezoelectric sensors can actually be put into practice as continuously distributed sensors, and on the other hand, because sensor arrays can be easily implemented by means of piezoelectric patches. In the present paper we are using the concept of spatial filters and their optimal approximation by

sensor arrays to design modal transducers for thin plates. Moreover, we include a paragraph, in which our method is compared to other methods reported in the literature.

As we have mentioned the proper distribution of the sensing and actuation is crucial for the control of continuous structures. Once the sensor and actuator systems have been properly designed the functioning of the communication between the structure and the controller is enabled and vibration control can be implemented. Typically, methods for vibration control are either passive (see Hagood and von Flotow 1991, Moheimani and Fleming 2006) or active (see e.g., Fuller *et al.* 1996, Preumont 2002). Concerning passive methods we mention piezoelectric shunt damping, which is the combination of passive electrical networks with piezoelectric patches attached to a mechanical structure. The resulting efficient damping system is autonomous of electrical sources, it guaranties stability and it is robust in case of variation of parameters at low weight and costs. Concerning active control modal control is one of the most commonly used approaches. In general modal control applies a transformation between physical and modal sensors and actuators, see Hanson and Snyder (1997) or Inman (1997), such that each mode can be controlled by one controller individually. Hence, modal transducers are combined with individual modal controllers. Although this concept has originally been designed for active vibration control it can as well be used in combination with passive shunt damping, in which spatial modal filters are used. The combination of spatial filters (in particular displacement filters) with shunt damping has recently been introduced by Schöftner and Irschik (2009) and Schöftner and Krommer (2012).

The present paper is concerned with the design of modal filters for thin plates, with the experimental verification of the resulting piezoelectric transducer arrays and with the application of the modal transducers for passive and active noise control of a test structure. It is structured as follows: In the first part of the paper the governing equations and the notation of the Kirchhoff plate theory are shortly summarized. Based on the concept of colocation the reader is introduced to the theory of spatial filters, such as modal and nilpotent filters. The theoretical investigations are demonstrated for a clamped rectangular plate. Next, an approximation of the continuously distributed modal transducers by a discrete sensor array is introduced. After complementing the theoretical part in section four with the description of the implemented experimental setup and the verification of the proposed design of the discrete piezoelectric transducer array, vibration control is the issue of the remaining part of the paper. A comparison of active modal control and passive shunt damping using the discrete piezoelectric transducer array for the reduction of vibrations and noise in plates is presented. Firstly, passive shunt damping is introduced and tuned *RL*-circuits are designed for damping the first three eigenmodes. Secondly, active modal control is considered. The control algorithm is designed for the first three eigenmodes. In the conclusion the paper is summarized and the benefits of the design of the discrete piezoelectric transducer array as well as the damping strategies are highlighted.

## **2. Problem formulation**

As we are studying the control of vibrations of a thin plate, we first introduce shortly the basic equations of thin plate theory, which serve as the basis for the design of distributed sensors and actuators. Throughout this part of the paper we use a direct tensor notation, which can be found in Lurie (2002) for three-dimensional problems; concerning the use of a direct tensor notation for thin plates we refer the reader to our own work (Krommer 2003), but also to the textbook by Selvadurai (2000), in which a notation very similar to the one used in the present paper can be

found.

For the case of pure bending of thin elastic plates in a geometrically linear regime we impose the Kirchhoff kinematical hypotheses (see the original paper by Kirchhoff (1850)); hence, we have the following set of governing equations: The balance equation

$$A: \quad \nabla \cdot \nabla \cdot \mathbf{M}(\mathbf{x}, t) + p_z(\mathbf{x}, t) = P \frac{d^2 w(\mathbf{x}, t)}{dt^2}, \tag{1}$$

which must be satisfied within the domain  $A$  of the plate for every point  $\mathbf{x}$  and at any time  $t > 0$ , the boundary conditions

$$\begin{aligned} \partial A: \quad & (\mathbf{M} \cdot \mathbf{n}) \cdot \mathbf{n} - \bar{m} = 0 \quad \text{or} \quad \nabla w \cdot \mathbf{n} = \bar{\psi}, \\ & (\nabla \cdot \mathbf{M}) \cdot \mathbf{n} + \nabla \cdot ((\mathbf{M} \cdot \mathbf{n}) \cdot \mathbf{s}) - \bar{q} = 0 \quad \text{or} \quad w = \bar{w}, \end{aligned} \tag{2}$$

which must be satisfied at the boundary  $\partial A$  and the conditions

$$P_i: [(\mathbf{M} \cdot \mathbf{n}) \cdot \mathbf{s}] = 0 \quad \text{or} \quad \omega = 0 \tag{3}$$

which must be satisfied for every point  $P_i$  of the boundary  $\partial A$ , at which the local coordinate system has a discontinuity; hence, where the unit normal and tangential vectors  $\mathbf{n}$  and  $\mathbf{s}$  are discontinuous.  $[ \ ]$  stand for the jump of an entity at the point  $P_i$  of the boundary. A sketch of the plate is shown in Fig. 1.

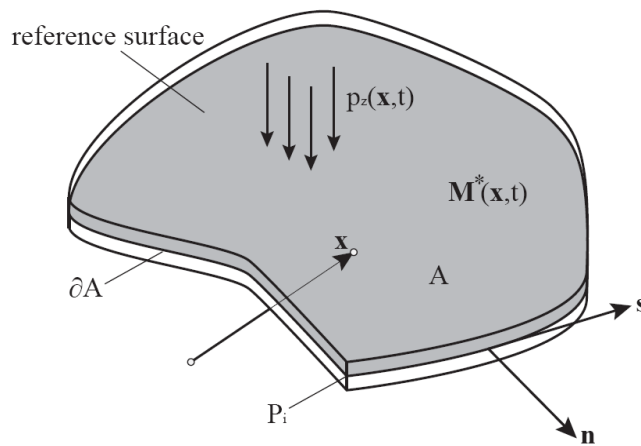


Fig. 1 Sketch of a thin plate with reference surface  $A$ , boundary  $\partial A$  and discontinuity point  $P_i$  at the boundary

In the above equations  $\nabla$  is the invariant two dimensional differential operator in the plane of the plate.  $\mathbf{M}(\mathbf{x}, t)$  is the plane second rank moment tensor,  $\nabla \cdot \mathbf{M}(\mathbf{x}, t) = \mathbf{Q}(\mathbf{x}, t)$  stands for the divergence of  $\mathbf{M}(\mathbf{x}, t)$ , which is balanced by the transverse shear vector  $\mathbf{Q}(\mathbf{x}, t)$  and  $\nabla \cdot \nabla \cdot \mathbf{M}(\mathbf{x}, t)$  is the divergence of the transverse shear vector, the sum of which with the distributed external

transverse force loading  $p_z(\mathbf{x},t)$  is balanced by the inertia force.  $P$  denotes the mass per unit area and  $w(\mathbf{x},t)$  stands for the transverse deflection.  $\bar{m}$  and  $\bar{q}$  are prescribed values for the normal moment and the Kirchhoff shear force at the boundary, and  $\bar{w}$  and  $\bar{\psi}$  are prescribed deflection and normal derivative of the latter in case of inhomogeneous kinematical boundary conditions.

The symmetric moment tensor is related to the symmetric second rank tensor of linearized curvatures  $\boldsymbol{\kappa} = -\text{sym}(\nabla\nabla w)$  by means of the constitutive relation

$$\mathbf{M} = \mathbf{D} \cdot \cdot \boldsymbol{\kappa} - \mathbf{M}^* . \tag{4}$$

$\mathbf{D} \cdot \cdot \boldsymbol{\kappa}$  stands for the double contraction of the fourth rank tensor of plate stiffnesses  $\mathbf{D}$  and the second rank tensor of linearized curvatures  $\boldsymbol{\kappa}$  (see e.g., Bonet and Wood (2008) for the corresponding notation used in a three-dimensional formulation).  $\mathbf{M}^*$  is a tensor, which characterizes a source of self-stress, which includes effects of non-mechanical sources; e.g., thermal expansion strains or piezoelectric strains that can be used to actuate the plate. The notion of sources of self-stress dates back to the first half of the 20<sup>th</sup> century and was introduced by Reissner (1931), Nemenyi (1931); more recent discussions can be found e.g., in Mura (1987) or Irschik and Ziegler (1988). Here, we also denote this tensor as actuation tensor. If it is separable in space and time, we introduce this separation as  $\mathbf{M}^*(\mathbf{x},t) = \mathbf{S}^a(\mathbf{x})f(t)$ , in which  $\mathbf{S}^a(\mathbf{x})$  is the actuator shape tensor characterizing the spatial distribution of the actuation and  $f(t)$  is the time variation of the actuation.

The set of governing equations is completed by introducing a sensor equation in the form of a strain-induced sensor as

$$y(t) = \int_A \mathbf{S}^s(\mathbf{x}) \cdot \cdot \boldsymbol{\kappa} dA. \tag{5}$$

Here,  $\mathbf{S}^s(\mathbf{x}) \cdot \cdot \boldsymbol{\kappa}$  denotes the double contraction of the second rank sensor shape tensor  $\mathbf{S}^s(\mathbf{x})$  and the tensor of linearized curvatures  $\boldsymbol{\kappa}$ . Such a sensor relation holds e.g. for the case of piezoelectric sensors. The sensor shape tensor represents the distribution of the sensing authority throughout the plate domain  $A$ . If  $\mathbf{S}^s(\mathbf{x}) = \mathbf{S}^a(\mathbf{x})$  holds, actuation and sensing are called collocated; for details concerning the notion of collocation we refer to Preumont (2002), Kugi (2001).

### 3. Modal sensors and actuators

In the following we focus our attention on collocated shape tensors; hence, on cases, for which  $\mathbf{S}^s(\mathbf{x}) = \mathbf{S}^a(\mathbf{x}) = \mathbf{S}(\mathbf{x})$ .  $\mathbf{S}(\mathbf{x})$  is denoted as shape tensor, which we assume symmetric. In case of sensors, the signal can be reformulated according to

$$y(t) = - \int_A \mathbf{S}(\mathbf{x}) \cdot \cdot \nabla\nabla w(\mathbf{x},t) dA. \tag{6}$$

Applying the Gauss integral theorem twice, we obtain

$$\begin{aligned}
 y(t) = & - \int_A \underbrace{\nabla \cdot \nabla \cdot \mathbf{S}(\mathbf{x})}_{=-p_z^d(\mathbf{x})} w(\mathbf{x}, t) dA + \int_{\partial A} \underbrace{\left( (\nabla \cdot \mathbf{S}) \cdot \mathbf{n} + \nabla \left( (\mathbf{S} \cdot \mathbf{n}) \cdot \mathbf{s} \right) \right)}_{=\bar{q}^d(\mathbf{x})} w(\mathbf{x}, t) dS \\
 & - \int_{\partial A} \underbrace{(\mathbf{S} \cdot \mathbf{n}) \cdot \mathbf{n}}_{=\bar{m}^d(\mathbf{x})} (\nabla w(\mathbf{x}, t) \cdot \mathbf{n}) dS.
 \end{aligned} \tag{7}$$

Here, we consider problems with homogenous kinematical boundary conditions, such that only those parts of the boundary, for which dynamical boundary conditions apply, say  $\partial A_m$  and  $\partial A_q$ , are kept in the above integrals. In order to assign a mechanical interpretation to the signal, we introduce a problem, through which the shape tensor is related to statically admissible stress tensors due to force loadings. It follows directly from Eq. (7) as

$$\begin{aligned}
 A : \quad & \nabla \cdot \nabla \cdot \mathbf{S} + p_z^d = 0 \\
 \partial A_m : \quad & (\mathbf{S} \cdot \mathbf{n}) \cdot \mathbf{n} = \bar{m}_d \\
 \partial A_q : \quad & (\nabla \cdot \mathbf{S}) \cdot \mathbf{n} + \nabla \left( (\mathbf{S} \cdot \mathbf{n}) \cdot \mathbf{s} \right) \cdot \mathbf{s} = \bar{q}^d
 \end{aligned} \tag{8}$$

in which the distribution of the static forces  $p_z^d(\mathbf{x})$ ,  $\bar{q}^d(\mathbf{x})$  and  $\bar{m}^d(\mathbf{x})$  is arbitrary. Then, the signal of the sensor is

$$y(t) = \int_A p_z^d(\mathbf{x}) w(\mathbf{x}, t) dA + \int_{\partial A_q} \bar{q}^d(\mathbf{x}) w(\mathbf{x}, t) dS - \int_{\partial A_m} \bar{m}^d(\mathbf{x}) (\nabla w(\mathbf{x}, t) \cdot \mathbf{n}) dS. \tag{9}$$

Hence, a proper choice of the static forces finds a sensor, the signal of which is the work conjugate to these forces. An overview discussing different choices of them has been given by Krommer and Irschik (2007) in a three-dimensional context. Clearly, Eq. (9) constitutes a spatial filter, whose ability to filter certain spatial information strictly depends on the choice of the static forces.

A classical example for such a spatial filter is a modal filter, which was introduced by Lee and Moon (1990). It is put into practice by a shape tensor, for which the signal filters the  $i$ -th modal coordinate  $A_i(t)$  from the total deflection  $w(\mathbf{x}, t) = \sum_{i=1}^{\infty} W_i(\mathbf{x}) A_i(t)$ ; here,  $W_i(\mathbf{x})$  is the  $i$ -th eigenmode of the plate. The corresponding eigenvalue problem is governed by

$$P \omega_i^2 W_i = \nabla \cdot \nabla \cdot \left( \mathbf{D} \cdot \text{sym}(\nabla \nabla W_i) \right), \tag{10}$$

in which  $\omega_i$  is the  $i$ -th eigenfrequency. Keeping in mind that the eigenmode must satisfy homogenous dynamical boundary condition at  $\partial A_q$  and  $\partial A_m$ , namely that  $\bar{q}_i = 0$  and  $\bar{m}_i = 0$ , we assume static forces in Eq. (8), such that

$$\begin{aligned}
 A : \quad & \nabla \cdot \nabla \cdot \mathbf{S}_i + \underbrace{\nabla \cdot \nabla \cdot \left( \mathbf{D} \cdot \text{sym}(\nabla \nabla W_i) \right)}_{=P \omega_i^2 W_i} = 0, \\
 \partial A_m : \quad & (\mathbf{S}_i \cdot \mathbf{n}) \cdot \mathbf{n} = 0, \\
 \partial A_q : \quad & (\nabla \cdot \mathbf{S}_i) \cdot \mathbf{n} + \nabla \left( (\mathbf{S}_i \cdot \mathbf{n}) \cdot \mathbf{s} \right) \cdot \mathbf{s} = 0
 \end{aligned} \tag{11}$$

holds. Then, the signal of the sensor is

$$y(t) = \int_A P \omega_i^2 W_i w(\mathbf{x}, t) dA = A_i(t). \quad (12)$$

Here, the eigenmodes have been assumed to be orthonormalized with respect to the linear inertia  $P$  times the eigenfrequency  $\omega_i^2$ . Hence, a modal filter is obtained. The shape tensor  $\mathbf{S}_i$  is computed from Eq. (11); yet, we note that the solution to this latter problem is not unique, as boundary conditions must only be satisfied at those parts of the boundary with dynamical boundary conditions. At the rest, no boundary conditions must be satisfied. Shape tensors  $\mathbf{S}^{nil}(\mathbf{x})$ , which are responsible for this non-uniqueness are called *nilpotent*. In general, nilpotent shape tensors exist for redundant plates only and the signal of a sensor put into practice by means of a nilpotent sensor shape tensor is always trivial. If a nilpotent shape tensor is used as an actuator shape tensor it produces no deflection, but only moments. For a detailed discussion of nilpotent sensors and actuators for beams we refer to Irschik *et al.* (1998).

A straightforward solution for the modal shape tensors is

$$\mathbf{S}_i = -\mathbf{D} \cdot \text{sym}(\nabla \nabla W_i) = \mathbf{M}_i. \quad (13)$$

Hence, the shape tensor is taken as the negative modal moment tensor  $\mathbf{M}_i$ . Modal filters are very well known types of spatial filters and are widely used in vibration control (e.g., Lee and Moon 1990 or Donoso and Bellido 2009), but also in the context of structural health monitoring, as introduced by Deraemaeker and Preumont (2006).

Shape tensors for modal actuators are identical, which follows directly from collocation; for more details in the three dimensional case we refer to Krommer and Irschik (2007). The modal shape tensor as introduced in Eq. (13) is of particular interest. If it is used as an actuation,  $\mathbf{M}^*(\mathbf{x}, t) = \mathbf{S}_i(\mathbf{x}) f(t) = \mathbf{M}_i(\mathbf{x}) f(t)$ , with a constant time variation  $f(t)$ , a deflection identical to an eigenmode  $w(\mathbf{x}, t) = W_i(\mathbf{x})$  is produced, but no stresses are induced. Such self-stress tensors are called *impotent* in the literature, see e.g., Mura (1987). In general, any self-stress tensor (in the context of thin plate theory rather self-moment tensor) can be uniquely decomposed into a nilpotent and an impotent part; a detailed discussion concerning this decomposition can be found in Nyashin *et al.* (2005). In other words, we can compute all possible modal self-stress tensors from

$$\mathbf{S}_i = \underbrace{-\mathbf{D} \cdot \text{sym}(\nabla \nabla W_i(\mathbf{x}))}_{=\mathbf{S}_i^{imp}(\mathbf{x})} + \sum_{j=1}^{\infty} \alpha_j \mathbf{S}_j^{nil}(\mathbf{x}) = \mathbf{S}_i^{imp}(\mathbf{x}) + \sum_{j=1}^{\infty} \alpha_j \mathbf{S}_j^{nil}(\mathbf{x}). \quad (14)$$

Here,  $\mathbf{S}_i^{imp}$  refers to the impotent modal shape tensor and  $\mathbf{S}_j^{nil}$  is any of the generally infinitely many nilpotent shape tensors.

**Clamped rectangular plate** As an example, we consider a rectangular acryl plate with all four edges clamped. The dimensions of the plate  $a \times b$  are 0.76 m  $\times$  0.56 m. We assume isotropic material behavior, such that we have a plate stiffness  $D = 357.4 \text{ Nm}$  and a linear inertia  $P = 11.81 \text{ kgm}^{-2}$ . For rectangular plates we introduce a notion, for which two indices are used to identify an eigenmode  $W_{ij}$ . In this case the governing equations for the eigenmodes follow from Eq. (10) as

$$\lambda_{ij}^4 W_{ij} = \Delta \Delta W_{ij}, \quad (15)$$

in which the eigenvalue  $\lambda_{ij}^4 = (P/D)\omega_{ij}^2$  has been introduced. For the isotropic plate under

consideration we consider the shape tensor spherical,  $\mathbf{S}_{ij} = S_{ij}\mathbf{I}$ , such the statically admissible shape function  $S_{ij}$  is then computed as any solution of

$$\Delta(S_{ij} + \Delta W_{ij}) = 0. \tag{16}$$

Note that the plate stiffness  $D$  is omitted in the above relation. No boundary conditions must be satisfied, because all boundary conditions are purely kinematical. Therefore, a straightforward solution is  $S_{ij} = -\Delta W_{ij}$ . The results for the distribution of these modal shape functions for the first three eigenmodes are shown in Fig. 2. Note that we used Finite Differences to compute these solutions; this is done throughout the paper as far as solutions are concerned with plates.

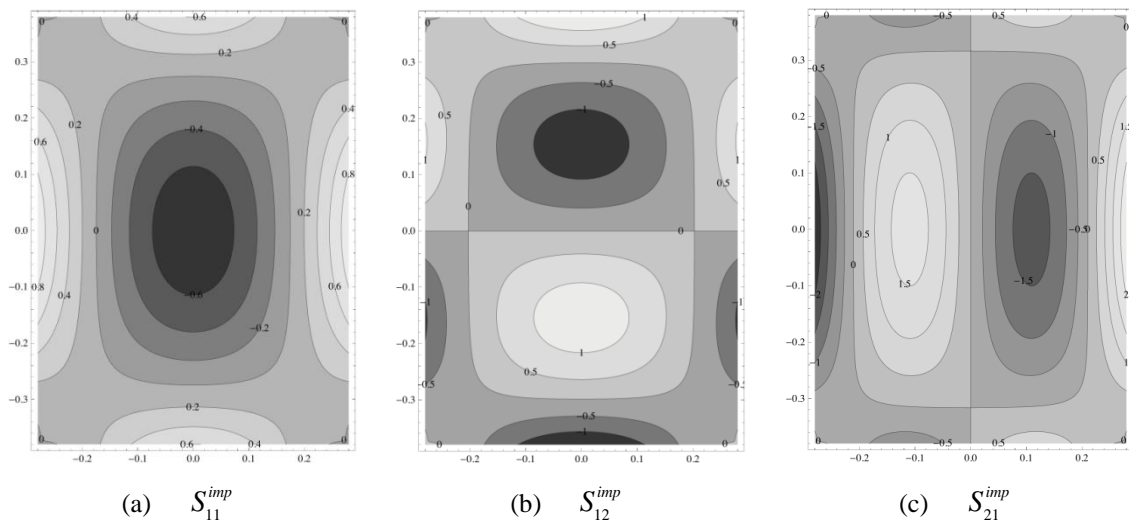


Fig. 2 Impotent modal shape functions

Moreover, these shape functions correspond to impotent shape tensors. Nilpotent shape tensors are computed by first computing alternative modal shape functions, which are solutions of

$$\begin{aligned} A: \quad & \Delta S_{ij} + \lambda_{ij}^4 W_{ij} = 0, \\ \partial A: \quad & S_{ij} = 0. \end{aligned} \tag{17}$$

The resulting modal shape functions are shown in Fig. 3. Computing the difference between corresponding shape functions taken from the two sets of solutions for modal shape functions must therefore lead to a set of shape functions, which are nilpotent; the latter either measure a trivial signal independent of the actual deformation, or, if used as actuator shape functions, they produce no deflection independent from the time variation the actuation is applied with. As mentioned before in the context of actuation only, nilpotent sensors and actuators have been studied by Irschik *et al.* (1998) and Krommer and Irschik (2007). The results for the nilpotent shape functions are presented in Fig. 4.

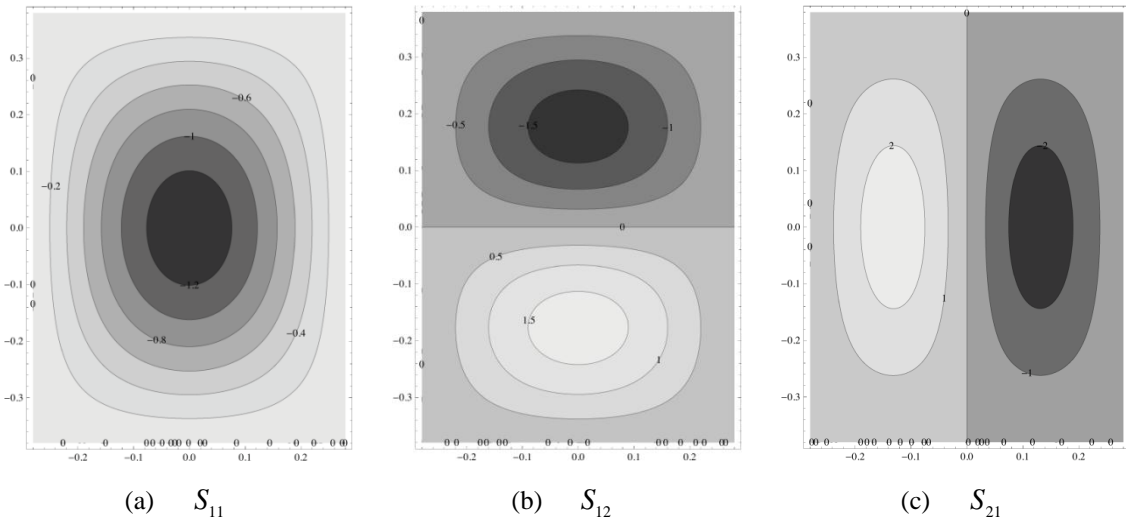


Fig. 3 Alternative modal shape functions

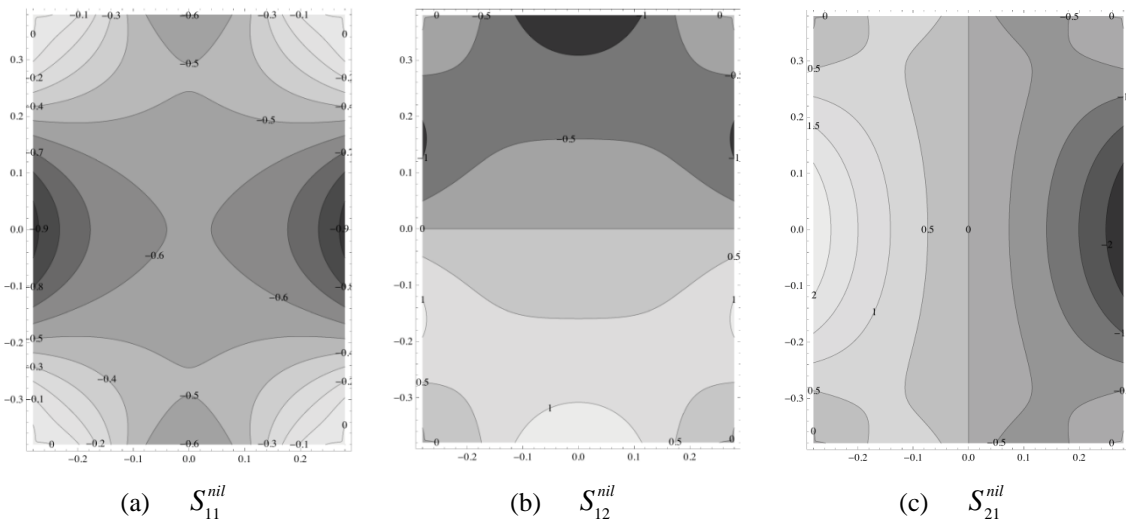


Fig. 4 Nilpotent shape functions

These nilpotent shape functions can be superposed upon any of the two sets of modal shape functions without changing the characteristics of neither the actuation nor the measured signal. In this paper we seek in particular for a superposition, for which the intensity of the shape function is low in the center of the plate and high in the vicinity of the edges.

### 3.1 Sensor / actuator array design

In many practical problems a distributed sensing or actuation by means of shape tensors cannot be put into practice - it rather must be approximated by an array of discrete sensors and actuators. For that sake we introduce a simple method to compute the locations and the individual intensities of the discrete sensors and actuators.

The plate domain  $A$  is decomposed into  $k = 1, \dots, n$  sub-domains with area  $A_k$ . In each sub-domain we compute the tensor valued 0<sup>th</sup> order moment  $\mathbf{S}_{ij,k}^0$  of the shape tensor  $\mathbf{S}_{ij}(\mathbf{x})$  as

$$\mathbf{S}_{ij,k}^0 = \int_{A_k} \mathbf{S}_{ij}(\mathbf{x}) dA, \tag{18}$$

and a vector valued 1<sup>st</sup> order moment  $\mathbf{s}_{ij,k}^1$  from

$$\mathbf{s}_{ij,k}^1 = \int_{A_k} \mathbf{S}_{ij}(\mathbf{x}) \cdot \mathbf{x} dA \tag{19}$$

Within each sub-domain one discrete sensor or actuator is located; the latter has a constant shape tensor  $\mathbf{S}_k = \text{const.}$ , an intensity center  $\mathbf{x}_k$ , and it covers the domain  $A_k$ , which is a sub-domain of  $A$ . We enforce the moments of the discrete distributions to be identical to the ones of the shape tensors, such that we find  $(3 + 2)n$  relations

$$\mathbf{S}_k \bar{A}_k - \mathbf{S}_{ij,k}^0 = 0 \text{ and } \mathbf{S}_k \mathbf{x}_k = \mathbf{s}_{ij,k}^1 = 0 \tag{20}$$

from which the constant shape tensors  $\mathbf{S}_k$  and the locations  $\mathbf{x}_k$  can be computed for a given shape tensor  $\mathbf{S}_{ij}(\mathbf{x})$ . The proposed simple method for the approximation of the distributed shape tensors is a straightforward extension of a method previously developed for sensor array design for beams by Krommer *et al.* (2009). We can use the method for approximating a modal sensor or actuator by an array of discrete sensors and actuators.

**Clamped rectangular plate** As an example we use the three modal shape functions for the rectangular clamped plate. For spherical shape tensors, we replace Eq. (20) by

$$S_k \bar{A}_k - \int_{A_k} S_{ij}(\mathbf{x}) dA = 0 \text{ and } \mathbf{x}_k \int_{A_k} S_{ij}(\mathbf{x}) dA - \int_{A_k} S_{ij}(\mathbf{x}) \mathbf{x} dA = \mathbf{0}, \tag{21}$$

which represents three equations for each of the  $k = 1, \dots, n$  sub-domains. We further note that any modal shape function can be written as

$$S_{ij}(\mathbf{x}) = S_{ij}^{imp}(\mathbf{x}) + \sum_{k,l} \alpha_{kl} S_{kl}^{nil}(\mathbf{x}); \tag{22}$$

due to the symmetry properties of the problem of a homogenous rectangular plate only those nilpotent shape functions, to which the same symmetry conditions as for the corresponding impotent modal shape function apply, are used in Eq. (22); e.g., for  $i$  odd and  $j$  odd,  $k$  and  $l$  should both be odd.

The superposition of nilpotent shape functions results into additional degrees of freedom  $\alpha_{kl}$  that can be used in the design of an array of discrete sensors and actuators approximating the distributed ones. As an example we consider the design shown in Fig. 5. We decompose the plate domain into 8 triangular sub-domains with equal area. Within each of the 8 sub-domains 1 group of sensors/actuators is attached. From the symmetries of the problem we conclude that studying a quarter of the plate with two triangular sub-domains is sufficient. In particular we consider the

right upper quarter and denote the upper triangle as domain 1 and the lower one as domain 2, see Fig. 5.

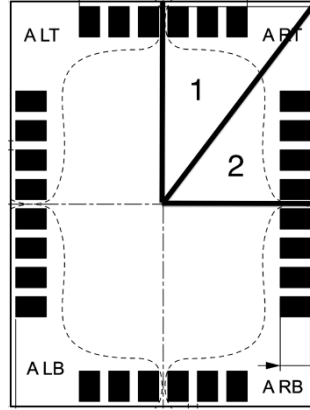


Fig. 5 Sensor/actuator array design with sub-domains

In both domains the location of the discrete array and the covered area are fixed, but the intensities are not. In particular the ratio between the two areas is  $\frac{\bar{A}_2}{\bar{A}_1} = \frac{4}{3}$  according to the number of individual constituents representing the discrete actuator/sensor within each sub-domain. Hence, only one unknown intensity remains in the 3 equations, Eq. (21), for each of the two sub-domains. To still compute a solution of Eq. (21) for the two sub-domains, we use 4 nilpotent shape functions superposed upon each of the impotent modal shape functions in Eq. (22). In particular, we consider the first three modal shape functions; here, we have

$$\begin{aligned} S_{11} &= S_{11}^{imp} + \alpha_{11}S_{11}^{nil} + \alpha_{13}S_{13}^{nil} + \alpha_{31}S_{31}^{nil} + \alpha_{33}S_{33}^{nil}, \\ S_{12} &= S_{12}^{imp} + \alpha_{12}S_{12}^{nil} + \alpha_{14}S_{14}^{nil} + \alpha_{32}S_{32}^{nil} + \alpha_{52}S_{52}^{nil}, \\ S_{21} &= S_{21}^{imp} + \alpha_{21}S_{21}^{nil} + \alpha_{23}S_{23}^{nil} + \alpha_{41}S_{41}^{nil} + \alpha_{25}S_{25}^{nil} \end{aligned} \quad (23)$$

and

$$\begin{aligned} 3S_1 - \int_{A_1} S_{ij} dA = 0 \quad \text{and} \quad \mathbf{x}_1 \int_{A_1} S_{ij} dA - \int_{A_1} S_{ij} \mathbf{x} dA = \mathbf{0}, \\ 4S_2 - \int_{A_2} S_{ij} dA = 0 \quad \text{and} \quad \mathbf{x}_2 \int_{A_2} S_{ij} dA - \int_{A_2} S_{ij} \mathbf{x} dA = \mathbf{0}, \end{aligned} \quad (24)$$

with  $\mathbf{x}_1$  and  $\mathbf{x}_2$  fixed, see Fig. 5. In Table 1 we show the results computed from Eq. (24) for the constant intensities  $S_1$  and  $S_2$  normalized with respect to  $S_2$ .

Table 1 Intensities of modal sensor and actuator networks for the first three modes

	(11) - mode	(12) - mode	(21) - mode
$S_1 / 1$	1.17	2.68	0.69
$S_2 / 1$	1	1	1

Clearly, the intensities in the two domains are different; yet, in some practical problems further design constraints may apply. E.g. we assume the two intensities to be identical,  $S_1 = S_2 = S$  in Eq. (24). We do not add any more nilpotent shape functions, such that we have 6 equations from Eq. (24), but only 5 unknowns. We solve this problem by a least square method. Once we have a solution for  $S$  and for the coefficients  $\alpha_{kl}$ , we compute the optimal modal shape functions from Eq. (23). The results are shown in Fig. 6.

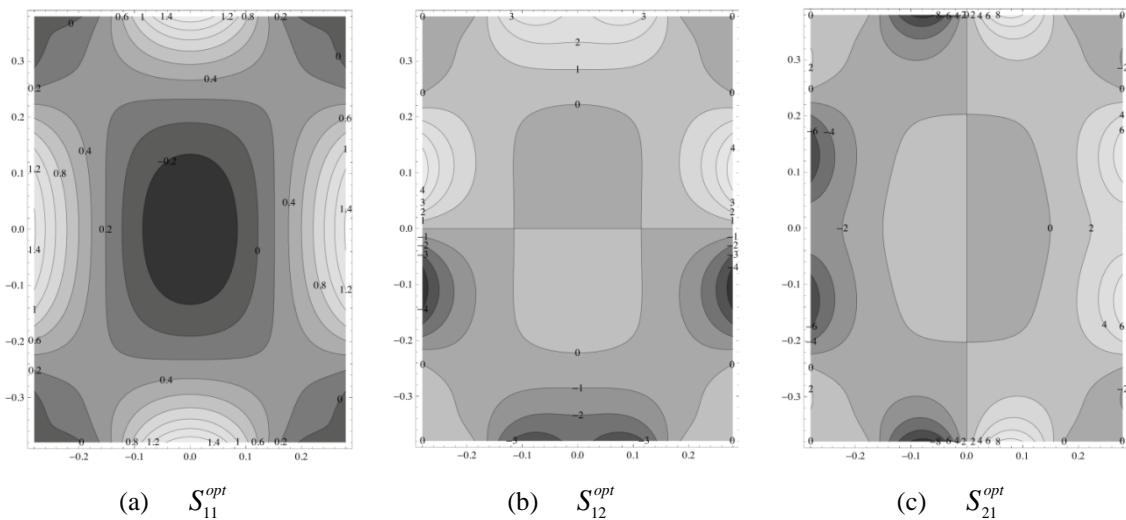


Fig. 6 Optimal modal shape functions

Table 2 Optimal intensities and locations of modal sensor and actuator networks for first three modes

	(11) - mode	(12) - mode	(21) - mode	actual design
$S_1 / N$	1	1	1	1
$S_2 / N$	1	1	1	1
$x_1 / m$	0.087	0.087	0.087	0.087
$y_1 / m$	0.349	0.359	0.340	0.345
$x_2 / m$	0.244	0.236	0.247	0.245
$y_2 / m$	0.116	0.116	0.116	0.116

Also, we recompute the locations and intensities by plugging these optimal shape functions into Eq. (24); these results are presented in Table 2; the  $x$ -coordinate is pointing rightwards and the  $y$ -coordinate is pointing upwards with the coordinate center in the center of the plate.

Obviously, the proposed design from Fig. 6 represents a design, which is optimal for the approximation of the first three modal shape functions in the framework of the method presented in this paper. As we are using a least square method, the locations are not exact, but the deviation is within an acceptable range.

**Discussion** Within this section we have introduced a novel methodology to design transducer arrays to put modal transducers into practice. The methodology itself is however not restricted to the design of modal transducers, but it can be used for the design of arbitrary transducers for plates with arbitrary boundary conditions. Concerning sensors, any kinematical entity can be measured as long as it represents the work conjugate to a force entity. Such sensors are denoted as spatial filters in the literature (Lee and Moon 1990, Krommer and Irschik 2007, Preumont *et al.* 2005, Preumont *et al.* 2003, Deraemaeker and Preumont 2006) and they can be put into practice either by continuously distributed sensors or approximated by arrays of dense sensors. Concerning actuators, any actuation that produces a displacement identical to the one induced by external forces can be put into practice. The design of such actuators is typically referred to as shape control (Irschik *et al.* 2003, 1999, Yu *et al.* 2009, Gattringer *et al.* 2003, Nader *et al.* 2003, Krommer and Varadan 2005, Tzou and Hollkamp 1994, Irschik 2002). Likewise to sensors, actuators are realized either continuously distributed or by means of dense actuator arrays.

Our methodology is based on the computation of the distribution of a continuously distributed transducer in a first step; then, we seek to approximate the continuous distribution using a transducer array. In the second step, we have only used a small number of individual constituents to the transducer array and computed the weights and locations of these individual transducers from an optimization procedure, for which the proper superposition of continuously distributed nilpotent transducers was advantageously applied. Hence, we were able to approximate the continuous distribution of a modal transducer with a transducer array using only a small number of individual transducers and, moreover, include an additional design constraint involving the possible locations of the transducers.

As the proposed method has been used in the context of only a small number of transducers, it is near at hand to shortly discuss other methods, which target at the same type of problems. Here, we refer to Gupta *et al.* (2010), who have reported on the various optimization criteria that are known in the literature for such problems; e.g., maximizing the modal forces/moments applied by piezoelectric actuators, minimizing the control effort/maximizing the energy dissipated, maximizing the degree of controllability or observability and minimizing spill-over effects. In the latter reference an exhaustive list of references is included; for instance, Hac and Liu (1993) proposed to use the observability/controllability Grammian matrix as a measure of observability/controllability. Transducer locations are then obtained such that selected eigenvalues of the observability/controllability Grammian matrix corresponding to the desired modes are maximized (Bruant and Proslie 2005). However, most of the methods discussed in Gupta *et al.* (2010) are targeted at modal transducers, and not at general transducers; hence, the present method is more general. This is also true concerning boundary conditions, which are arbitrary for the present method, but which are restricted to cantilevered or simply supported smart plate structures in the paper by Gupta *et al.* (2010). Concerning the study of clamped plates, which is the example problem used in the present paper we refer e.g., to Hwang *et al.* (1997) and Ma (2003), in which the transducers are not located along the clamped boundaries, but in the interior of the plate, which would not be suitable for our problem. A simple method, which is related to the present one is to place the transducers at the locations of the maximum modal strains. However, if one uses modal strains rather than modal stresses (as in the present paper) as a criterium for transducer placement,

the superposition of nilpotent distributions is no longer possible, because such distributions do not exist in the context of strain, but only in the context of stress. This would result into optimal placements, which are not restricted to the vicinity of the boundaries. Again, we point out the superiority of our method based on stress distributions compared to methods based on strain distributions.

As a conclusion for this part of the paper, we note that our method is a general one; it can be used to design different types of transducer arrays, it can be applied to arbitrary boundary conditions and it works for both, a large number or a small number of individual transducers. Moreover, the criteria used for transducer placement and weight assignment can be further refined to extend the applicability to a broader frequency range; this has been done previously in Krommer *et al.* (2009) for beams. Within the present paper, where only four individual transducers are used such extensions are not possible; one would need a larger number of transducers to do so. In the following we will experimentally verify the proposed method and apply the obtained transducer array design for passive and active modal control of a thin plate structure.

#### 4. Experimental verification

In the present section, the experimental setup, to which the proposed theoretical approach will be applied, is presented. Due to the limitations of distributed sensors and actuators in real applications, piezoelectric sensors and actuators are put into practice with discrete piezoelectric patches. The dimensions of the experimental setup and the placement of the piezoelectric patches is specified. The resulting design of the modal sensor and actuator array is experimentally verified.

##### 4.1 Experimental setup

Sensors and actuators of type DuraAct A15 are attached to an acryl glass plate (PMMA with Young's modulus  $Y = 4530 \text{ Nmm}^{-2}$ , Poisson ratio  $\nu = 0.38$  and density  $\rho = 1181 \text{ kgm}^{-3}$ ) based on the results of the previous section (see Fig. 6 and Table 2) which were computed by accounting for several design constraints concerned with the location of the piezoelectric patches as well as with their intensities. The corresponding experimental setup is shown in Fig. 7(a). The piezoelectric patches are attached at the inner side of the plate. The plate itself has the dimensions  $562 \text{ mm} \times 762 \text{ mm} \times 10 \text{ mm}$  and it is fixed along its clamped boundary to a medium density fiberboard housing (MDF with Young's modulus  $Y = 2700 \text{ Nmm}^{-2}$ , Poisson ratio  $\nu = 0.41$  and density  $\rho = 695 \text{ kgm}^{-3}$ ). In Fig. 7(b) the details of the design of the sensor and actuator array are shown; 28 piezoelectric patches are attached in total. A loudspeaker is put into the housing in order to excite vibrations of the acryl plate and accordingly results into structure-borne sound outside the housing. The general goal of this experimental setup is to reduce this structure-borne sound.

First, we validate the plate model used in the previous section with experimental and numerical results; in particular, we compare the measured first three eigenfrequencies and eigenmodes with the computed ones, which do not account for the stiffening effect of the attached patches. In Table 3 the eigenfrequencies are presented, for which numerical results using Finite Elements, which take the influence of the housing and of the imperfect clamping into account, are shown as well (analytical refers to the Finite Difference thin plate solution). The Finite Element results were computed with the commercially available code Ansys<sup>®</sup>. The built-in mesh generator of Ansys<sup>®</sup>

was used to generate the Finite Element mesh of the system; this resulted into the use of 21389 solid186 (3D 20-Node Structural Solid) elements and 312 solid187 (3D 10-Node Tetrahedral Structural Solid) elements for the housing, 7340 solid186 elements and 12 solid187 elements for the acryl plate and 24 solid186 elements for each of the 24 piezoelectric patches. Electromechanical coupling due to the direct piezoelectric effect has not been taken into account in the Finite Element computations.

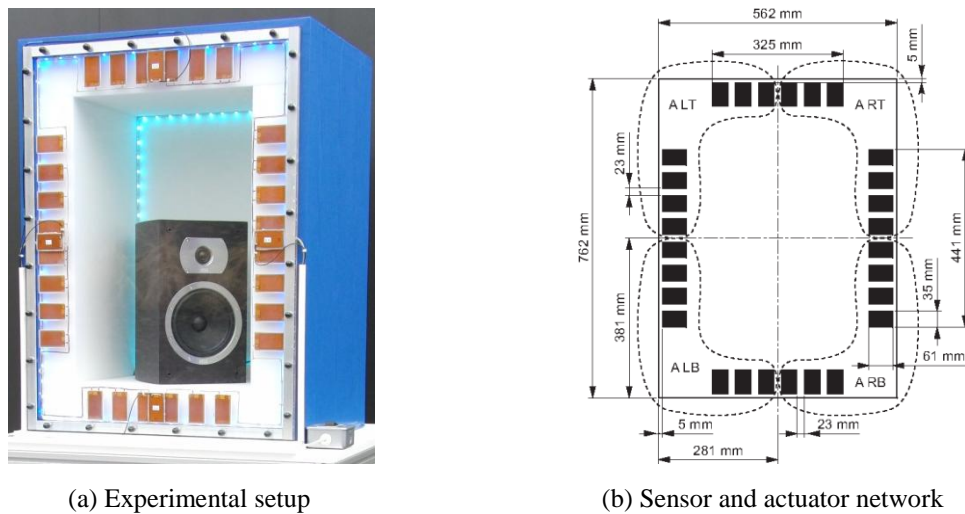


Fig. 7 Details of the plate

Table 3 Eigenfrequencies

	$f_{11} / \text{s}^{-1}$	$f_{12} / \text{s}^{-1}$	$f_{21} / \text{s}^{-1}$
measured	85	135	189
analytical	79.3	131.4	187.8
numerical	85.8	138.6	187.9

Fig. 8 shows the corresponding eigenmodes, which were either measured using a scanning laser vibrometer, computed with the Finite Elements or computed for the plate model. We conclude that the results computed using the model of an isotropic plate from the previous section are close enough to the measured results to base the network design problem on the plate model. In particular, because we can see that the acryl plate, which is fixed to the housing, behaves like a clamped plate in the frequency range that is of interest to us for the design of the piezoelectric transducer network.

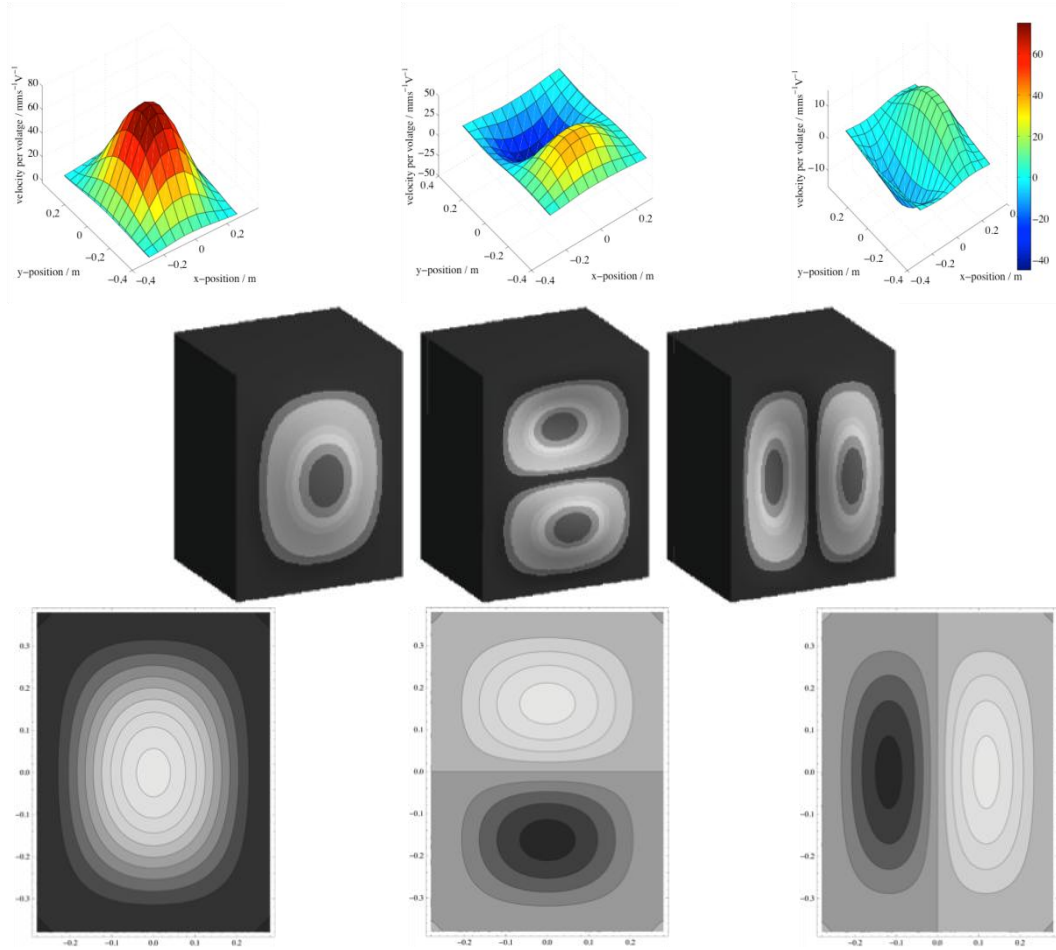


Fig. 8 Eigenmodes: top - measured, middle - finite elements and bottom - plate theory

#### 4.1.1 Sensor/actuator array verification

The details of the sensor/actuator array design are shown in Fig. 7(b). This design has been shown in the previous section to represent an approximation of the first three optimal modal shape functions, which are shown in Fig. 6. In particular, with respect to one quarter of the plate; the centers of the patch group with four patches and of the one with three patches are very close to the intensity centers of the three optimal modal shape functions, the ratio between the areas covered by these two groups is 4 / 3 and the intensities are identical. From these latter facts we conclude on the fact the 7 patches within each of the four quarters of the plate can be used in a parallel connection; the resulting four groups of 7 piezoelectric patches are denoted as *ALT*, *ART*, *ALB* and *ARB*, see Fig. 7(b).

Each of the four groups can be characterized by a so-called transducer equation

$$Q_k = C_p V_k + Q_k^m, \quad k = ALT, ART, ALB \text{ and } ARB, \quad (25)$$

in which  $Q_k$  is the total charge,  $C_p$  the combined capacity of the 7 patches,  $V_k$  the voltage and  $Q_k^m$

stands for the mechanical part of the total charge, see e.g., Krommer (2003). Denoting the area with three patches as  $\bar{A}_{k,1}$  and the one with four patches as  $\bar{A}_{k,2}$  this mechanical part of the total charge is defined as

$$Q_k^m = S_k \left( \int_{\bar{A}_{k,1}} \Delta w(\mathbf{x}, t) dA + \int_{\bar{A}_{k,2}} \Delta w(\mathbf{x}, t) dA \right), \quad (26)$$

because the intensity  $S_k$  is identical in the two groups. For the actuator mode the voltage  $V_k$  is applied, whereas for the sensor mode  $V_k$  is measured under open circuit conditions  $Q_k = 0$ . To put the first three modal sensors and actuators into practice by the array of piezoelectric patches the following rules, which are a direct result of the symmetry properties of these three modes, are applied:

- For the first mode all four groups are used in a parallel connection. For the actuator mode this results into the same voltage applied to all patches,  $V_{ALT} = V_{ART} = V_{ALB} = V_{ARB} = V$ , and for the sensor mode we have the total charge  $Q$ , which is zero for the open circuit conditions, as the sum of the four charges

$$Q = 0 = 4C_p V + (Q_{ALT}^m + Q_{ART}^m + Q_{ALB}^m + Q_{ARB}^m). \quad (27)$$

Hence, the measured voltage is proportional to the sum of all four mechanical parts of the total charge.

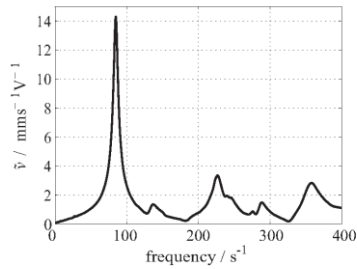
- For the second mode the two groups on the top are in a parallel connection, as are the two groups at the bottom; their connection however is anti-parallel. Hence, for the actuator mode we have  $V_{ALT} = V_{ART} = -V_{ALB} = -V_{ARB} = V$  and for the sensor mode  $0 = 4C_p V + (Q_{ALT}^m + Q_{ART}^m - Q_{ALB}^m - Q_{ARB}^m)$  holds.

- For the third mode the two groups on the right are in a parallel connection, as are the two groups on the left; their connection however is anti-parallel. Hence, for the actuator mode we have  $V_{ALT} = -V_{ART} = V_{ALB} = -V_{ARB} = V$  and for the sensor mode  $0 = 4C_p V + (Q_{ALT}^m - Q_{ART}^m + Q_{ALB}^m - Q_{ARB}^m)$  holds.

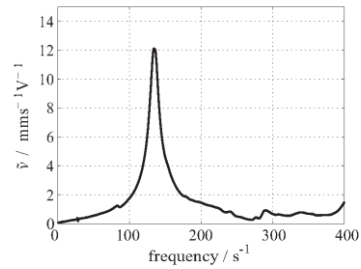
Accordingly, three operating modes corresponding to the first three eigenmodes can be realized for both, actuation and sensing. All the measurement results in this section have been obtained using a sine sweep excitation; either for the input voltage of the loudspeaker or for the voltage applied to the piezoelectric actuator array.

In Fig. 9 the amplitude spectra of  $\tilde{v}$ , which is the measured velocity of the plate per input voltage applied at the piezoelectric patches at  $x = 122$  mm and  $y = 175$  mm are shown for the case the piezoelectric patch array is used in its three actuator modes. The frequency range shown in the figures covers the first 8 eigenfrequencies of the plate. One can clearly see the ability of the actuator array to actuate a single mode; yet, the use of the array results into non ideal modal actuators, which can also be seen from the figure.

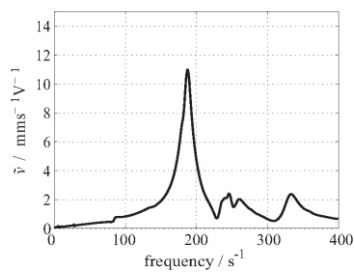
In Fig. 10 we show the measured amplitude spectra for using the array in its three operating modes as modal sensors; the plate is excited by the loudspeaker. The amplitude  $\tilde{V}$  denotes the output voltage of the piezoelectric patch per input voltage of the loudspeaker. One can see that our design approximately results into modal filters, as desired.



(a) Operating mode 1: (11) - mode

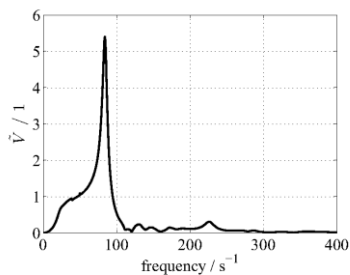


(b) Operating mode 2: (12) - mode

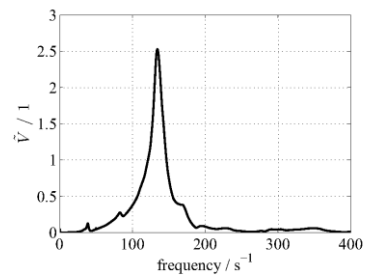


(c) Operating mode 3: (21) - mode

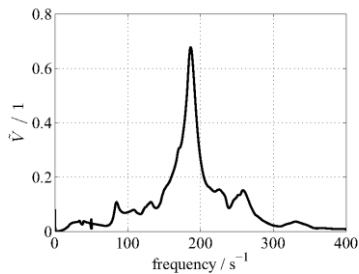
Fig. 9 Measured velocities due to modal actuation



(a) Operating mode 1: (11) - mode



(b) Operating mode 2: (12) - mode



(c) Operating mode 3: (21) - mode

Fig. 10 Measured modal voltages due to loudspeaker excitation

#### 4.1.2 Alternative sensor array

To facilitate active vibration control two arrays of piezoelectric patches would be needed. One could add a second array on the opposite side of the plate (in our case the outer side) made of 28 patches designed identical to the one implemented at the inner side of the plate. This would require a high number of additional patches as well as additional wiring. In order to avoid that, we use only four patches attached to the outer side of the plate, see Fig. 11, as an alternative sensor array, which is used for active vibration control.

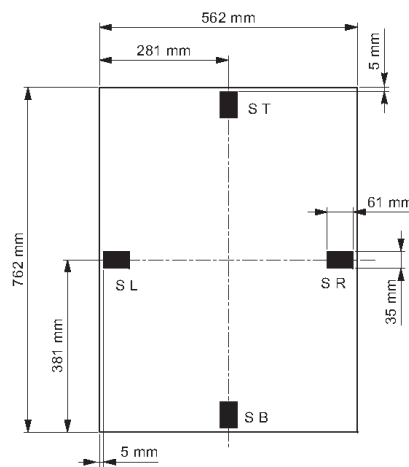


Fig. 11 Details of the alternative sensor array (Berger 2011)

The four sensor patches are attached in the middle of each lateral edge as near as possible to the clamping. The first three eigenmodes can be clearly identified by correct summation, which has been stated by Fuller *et al.* (1996) :

- Operating mode 1: Summation or parallel connection of all four sensors *SB*, *ST*, *SL* and *SR* leads to the measurement of the first mode, the second and the third mode are filtered out.
- Operating mode 2: Subtraction or anti-parallel connection of the bottom sensor *SB* and the top sensor *ST* to measure the second mode; the other two sensors are not active. The first and third mode are filtered out.
- Operating mode 3: Subtraction or anti-parallel connection of the left sensor *SL* and the right sensor *SR* (the other two sensors are not active) results into measuring only the third mode, whereas the first and second mode are filtered out.

The results for the alternative design for the modal sensor array using only the four sensor patches are shown in Fig. 12; the voltages at the piezoelectric patches are measured for the loudspeaker excitation.

Again the amplitude  $\tilde{V}$  denotes the output voltage of the piezoelectric patch per input voltage of the loudspeaker. Here, we can see that the signal levels are lower than for the original array with 28 patches due to the use of less sensors. Qualitatively, the results for the first and second mode are comparable; for the third mode the filtering ability is worse than for the original array with 28 patches. This can be attributed to the fact that the experimental setup does not exactly satisfy the symmetry conditions that would be required by the design of the alternative sensor array for

operating mode 3 to function better. Due to the use of only two sensor patches (*SL* and *SR*) small deviations from the ideal symmetry conditions can result into significant interference with the desired modal filtering ability. The two side peaks in Fig. 12(c) correspond to the (11) - mode and the (13) - mode of the acryl plate, which are symmetric with respect to the *y*-coordinate. From this fact we conclude on certain unsymmetries in the experimental setup for the modes that ideally would be symmetric with respect to the *y*-coordinate, but not for the modes that ideally would be symmetric with respect to the *x*-coordinate, because we have no such side peaks for operating mode 2.

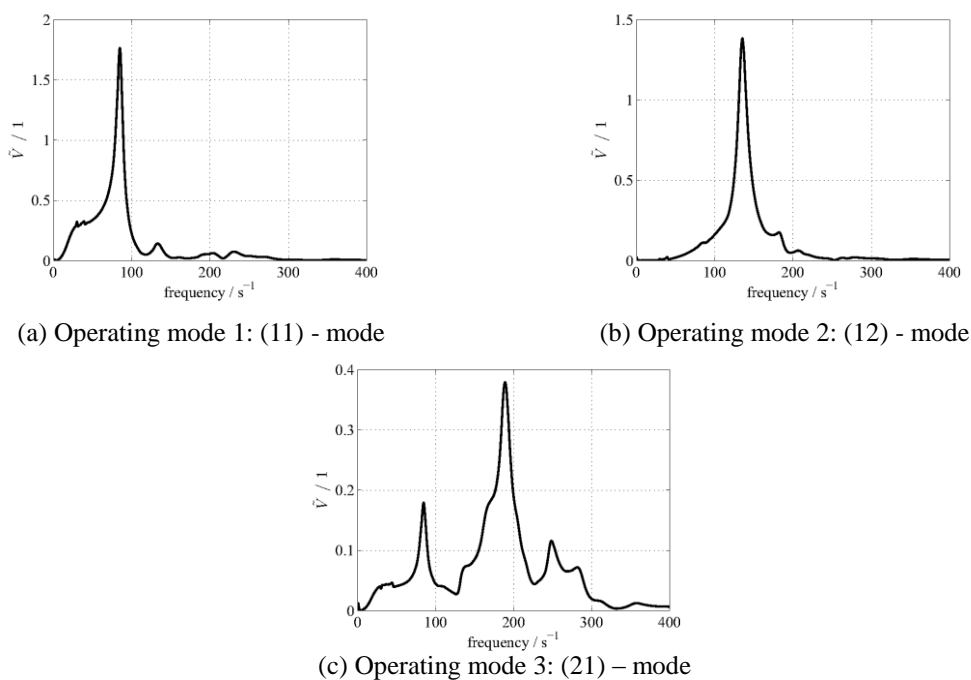


Fig. 12 Measured alternative modal voltages due to loudspeaker excitation

Although our design of the sensor and actuator arrays is only approximate, we conclude that it is sufficient for further use concerned with the control of the vibrations of the plate in the low frequency range. Concerning shunt damping the array with 28 patches, which works well as a sensor and as an actuator array, will be used and for active control the actuator array with 28 patches will be used in combination with the sensor array with 4 patches; in this latter case the deviations for operating mode 3 for the alternative sensor array will be compensated by the proper functionality of the actuator array for this operating mode.

## 5. Vibration control

On our experimental setup, two different vibration control techniques are implemented to proof

the efficiency of the design of the modal sensor and actuator arrays. The two control strategies are shortly introduced in the following without going into any detail, as this would go beyond the scope of this paper. Experimental results for the controlled plate structure will conclude the present paper.

### 5.1 Piezoelectric shunt damping

Piezoelectric shunt damping is a common and popular method to damp vibrations in elastic thin structures such as beams and plates. An electrical circuit is connected to the piezoelectric patches, which are attached to the mechanical structure to be damped. This damping method uses the patches as sensors as well as actuators at the same time and has been introduced by Hagood and von Flotow (1991). It can be classified in active and passive methods and these moreover in linear and nonlinear techniques, see Moheimani and Fleming (2006) for further details.

In the present paper we focus on the most effective passive shunt damping devices, the so-called resonant circuits, which are independent of any additional sources and can be interpreted analogous to a tuned mass damper (see e.g., Den Hartog (1985)). Their design can be computed with the help of the equivalent electrical circuit of a piezoelectric transducer, which describes the electromechanical relations electrically with a current source  $I^m$ , the piezoelectric capacitance  $C_p$  as a function of the permittivity and the patch dimensions (see Moheimani and Fleming (2006) and Krommer (2003)), and the impedance  $Z$ , which represents the electrical networks; see Fig. 13 for a connected  $RL$  circuit.

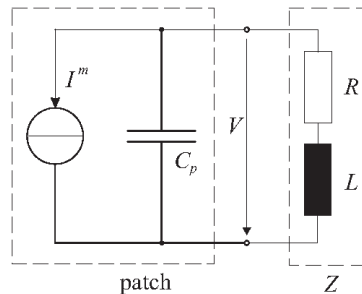


Fig. 13 Equivalent electrical circuit with  $RL$  shunt

In our problem we have the transducer equation

$$I_{ij} = 4C_p \dot{V}_{ij} + I_{ij}^m, \tag{28}$$

in which  $ij$  is either 11, 12 or 21. Here, we combine the design of the piezoelectric transducer array with 28 piezoelectric patches for the first three modes with shunt damping devices designed for the designated mode. We use single-mode  $RL$  circuits, which are designed to compensate one mode with the eigenfrequency  $\omega_{ij}$ ; the impedance of the electrical circuit in Fig. 13 is

$$Z = R + j\omega L. \tag{29}$$

With a known  $C_p$ , the essential inductance  $L$  can be expressed as

$$L = k \frac{1}{\omega_{ij}^2 (4C_p)}; \quad (30)$$

the inductance depends on the capacitance  $C_p$ , the eigenfrequency, for which the vibrations are meant to be damped and a factor  $k$  with an empiric value  $k \approx 0.995$ , which has been observed in many experiments, see Zenz (2011). Concerning the value of the eigenfrequency  $\omega_{ij}$  one must keep in mind that there exist two limiting cases for piezoelectric structures. (1) the short-circuit eigenfrequency for  $V = 0$  and (2) the open-circuit eigenfrequency for  $I = 0$ . Indeed, these two are different and the efficiency of shunt damping strongly depends on the gap between the two, which is normally characterized by the so-called electromechanical coupling coefficient (EMCC), see e.g., Trindade and Benjeddou (2009). In the present paper, the open-circuit eigenfrequency has been used in Eq. (30).

The proper value for the resistors  $R$  is crucial for the efficiency of the resonant circuit; if  $R$  is too small two resonant peaks close to the eigenfrequency to be controlled are observed and if  $R$  is too large the damping effect is reduced or, in the worst case, even lost. For  $R \rightarrow \infty$  open-circuit conditions are observed. As there is no correct analytical approach to determine the proper value, optimization techniques have to be used. A common challenge of resonant shunt circuits are the high values of the inductance. To avoid these huge components there are several options: The use of a large number of piezoelectric patches in parallel, additional parallel capacitances or the use of virtual or synthetic circuits. By using the modal transducer arrays in the present experimental setup we can avoid these large inductance values as all patches can be connected either parallel or anti-parallel, connecting the electrodes corresponding to the respective mode - in any case the total capacitance is 28 times the capacitance of a single patch.

As passive shunt damping devices are defined as circuits, for which no additional power is supplied to the system, stability of the shunted systems can be guaranteed, which has been extensively studied in the literature. For further details see e.g. Moheimani and Fleming (2006).

**Experimental results** The electrical components were determined experimentally as shown in Table 4 based on a first estimation using Eq. (30) and an optimization algorithm for the resistor values. All 28 patches are connected according to the three operating modes. Therefore attention has to be paid on the proper connection of the individual electrodes of the patches, or otherwise the damping effect is lost. In case of the first mode all patch groups are connected parallel, whereas for the second and third mode the corresponding patch groups are connected anti-parallel. For the second and third mode also alternative shunt circuits were considered where two independent resonant circuits are designed; in case of the second mode the electrodes at the top ( $ALT$ ,  $ART$ ) and the ones at the bottom ( $ALB$ ,  $ARB$ ) are used individually in a parallel connection. In case of the third mode the electrodes at the left ( $ALT$ ,  $ALB$ ) and the ones at the right ( $ART$ ,  $ARB$ ) are also connected correspondingly. Consequently two different capacitance values for the second and the third mode arise, the smaller value indicating the two independent circuits, see Table 4.

Table 4 Electric values of the shunt damping circuits

	(11) - mode	(12) - mode	(21) - mode	(12) - mode	(21) - mode
$C_p / \text{nF}$	1212	1212	1212	606	606
$L_{opt} / \text{H}$	2.87	1.18	0.583	2.33	1.166
$R_{opt} / \Omega$	170	110	70	160	100

The results for vibration reduction using the shunt circuits are shown in Fig. 14; in particular, the amplitude spectrum of the measured lateral velocity per unit voltage of the loud speaker, which is used for the excitation of the plate (by means of a sine sweep excitation), at the point  $x = 122$  mm and  $y = 175$  mm are shown. As a reference the results for short-circuited electrodes as well as an open-circuit are included.

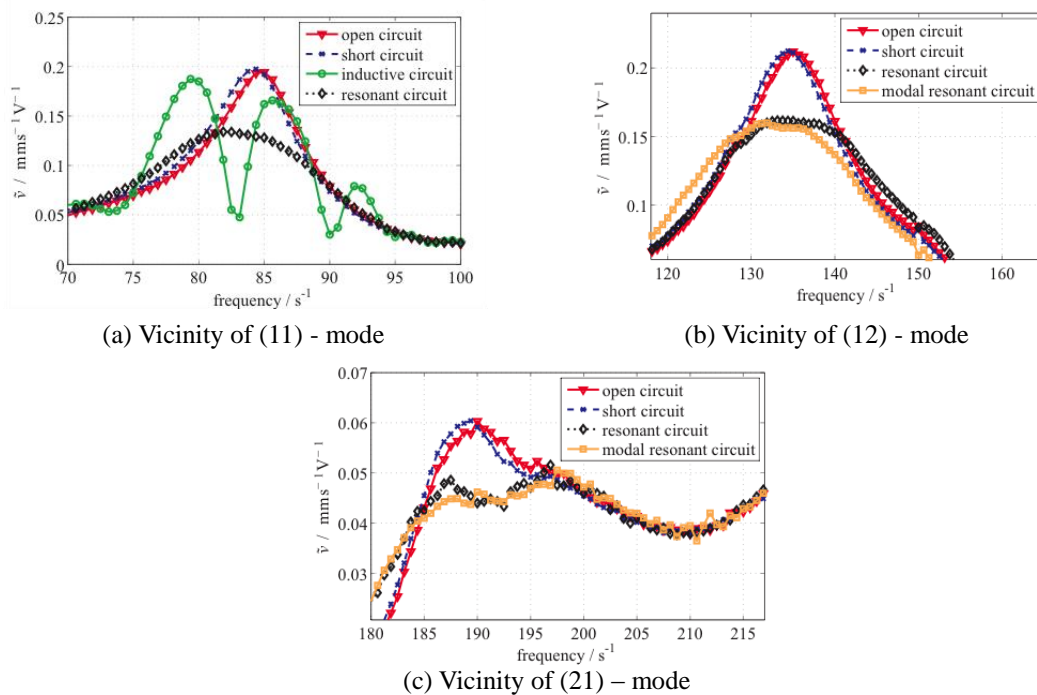


Fig. 14 Measured results for shunt damping

Using solely an inductance (inductive-circuit) the network almost annihilates the vibrations in a narrow spectrum, but typical resonance peaks of a vibration absorber occur beside this suppression, see Fig. 14(a), in which an inductive-circuit has been tested for the first mode. These side peaks can be avoided by introducing an additional resistor, though flattening the response such that the vibration reduction is reduced from  $-12.5\text{dB}$  to  $-3.5\text{dB}$  at the eigenfrequency. Figs. 14(b) and 14(c) show the effect of an optimally tuned resonant circuit on the second and third mode. The two types of circuits discussed above were realized. First the approach with two individual resonant  $RL$ -circuits was used (denoted as resonant circuit). Secondly, the transducer array was operated either in its second or third operating mode with only one  $RL$ -circuit for each mode (denoted as modal resonant circuit). The advantage of the second method is obvious. Only one circuit must be put into practice and furthermore a significantly smaller inductance values due to the doubled piezoelectric capacitance is needed, whereas the damping effectivity remains unchanged with a reduction of  $-2.5\text{dB}$ . Besides the reduction in dB, the modal damping ratio is of interest as well; Table 5 shows these ratios for the open-circuit conditions and for the single  $RL$ -circuits for each mode.

Table 5 Modal damping ratios

	(11) – mode	(12) – mode	(21) - mode
open-circuit	0.037	0.044	0.047
<i>RL</i> -circuit	0.074	0.075	0.07

Of course the observed reductions of the amplitudes are only valid at the measurement point. Measuring the reductions at the anti-node of each mode, where the maximum vibration amplitude is measured, a reduction of up to -23dB for an inductive circuit (*L*-circuit) and -5dB for an *RL*-circuit can be achieved. Multi-mode circuits could reduce the first three eigenmodes simultaneously. In this case one multi-mode shunt circuit for every group of the array (*ALT*, *ALB*, *ARB*, *ART*) must be designed, see Moheimani and Fleming (2006). The maximum achievable damping rate would be alike each separate single-mode circuit of Fig. 14, see Zenz (2011).

### 5.2 Active modal control

Generally speaking active modal control is a control approach, which can control each mode separately without affecting the others. Therefore each controller loop can be designed individually (Fuller *et al.* (1996)) due to the orthogonality of the eigenmodes. Based on the derivation of Hanson and Snyder (1997), Fuller *et al.* (1996), Preumont (2002) and Herold (2003) the local sensor signals can be written in terms of modal values; or in an inverse sense, the modal signals can be computed from the local sensor signals.

Our system consists of the vibrating plate itself and the attached sensors and actuators. Using the four local sensor signals as output, the three modal sensor signals, which are equal to the negative control error, can be computed from

$$\underbrace{\begin{bmatrix} y_{11} \\ y_{12} \\ y_{21} \end{bmatrix}}_{=y(t)=-e(t)} = \begin{bmatrix} 1 & 1 & 1 & 1 \\ 1 & -1 & 0 & 0 \\ 0 & 0 & 1 & -1 \end{bmatrix} \begin{bmatrix} y_{ST} \\ y_{SB} \\ y_{SL} \\ y_{SR} \end{bmatrix} \quad (31)$$

In the previous section we have validated this transformation experimentally, see Fig. 12. Here, the four local signals represent the measured voltages at the four patches shown in Fig. 11. The modal signals  $\mathbf{y}(t) = -\mathbf{e}(t)$  are fed into three individual modal controllers, which produce the three modal inputs  $\mathbf{u}(t)$  with  $u_{ij}(t) = f_{ij}(y_{ij}(t))$ , which have to be transformed from the modal space to the physical space. This transformation follows from the previous section as

$$\begin{bmatrix} u_{ALT} \\ u_{ART} \\ u_{ALB} \\ u_{ARB} \end{bmatrix} = \begin{bmatrix} 1 & 1 & 1 \\ 1 & 1 & -1 \\ 1 & -1 & 1 \\ 1 & -1 & -1 \end{bmatrix} \underbrace{\begin{bmatrix} u_{11} \\ u_{12} \\ u_{21} \end{bmatrix}}_{=u(t)} \quad (32)$$

As we have seen before, this transformation results into modal actuators, see Fig. 9. Note that in this control method the three modal controllers are designed individually; the effectiveness of

such an approach strongly relies on the functionality of the modal filtering capability. To verify this latter ability we show the measured amplitude spectrum of the nine modal transfer functions  $T_{y_{ij}/u_{kl}}$  with  $ij$  and  $kl$  equal to 11, 12 and 21 in Fig. 15, where a sine sweep excitation has been used for the actuator voltages and the sensor voltages have been measured.

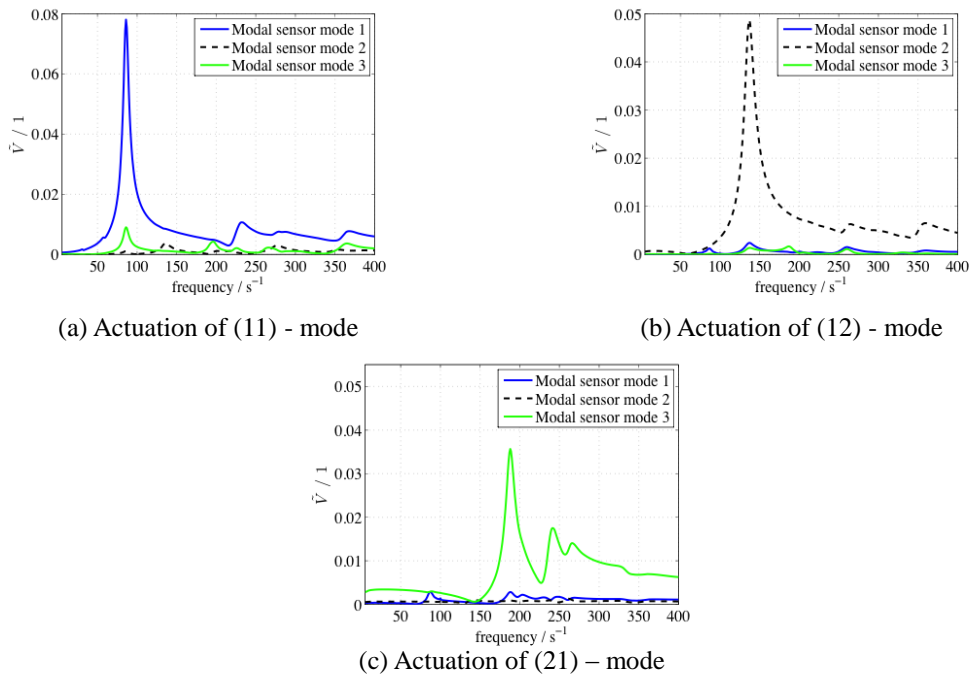


Fig. 15 Amplitude spectrum of transfer functions

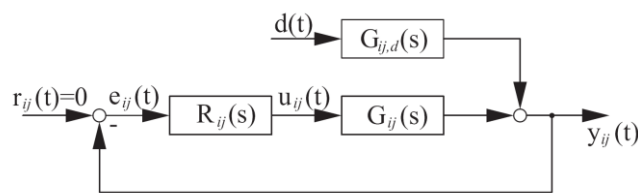


Fig. 16 Closed loop individual modal control (Berger 2011)

Hence, we conclude on the functionality of our sensor/actuator array design for modal control. To achieve an effective vibration control the piezoelectric patches were calibrated to balance possible deviations in between them resulting from diverse effects like variation of the patches, imprecise positioning, different intensity of the adhesive layer and also different material characteristics. The second peak in Fig. 15(c) can be contributed to these effects as well as to unsymmetries in general; see also the discussion at the end of section 4.1.2.

We can conclude from the results of Fig. 15 that the transfer matrix of the MIMO system with 3 modal inputs and 3 modal outputs is approximately diagonal. Therefore, we can design three individual controllers for the three modal transfer functions. The corresponding control scheme is shown in Fig. 16, see also Berger (2011).

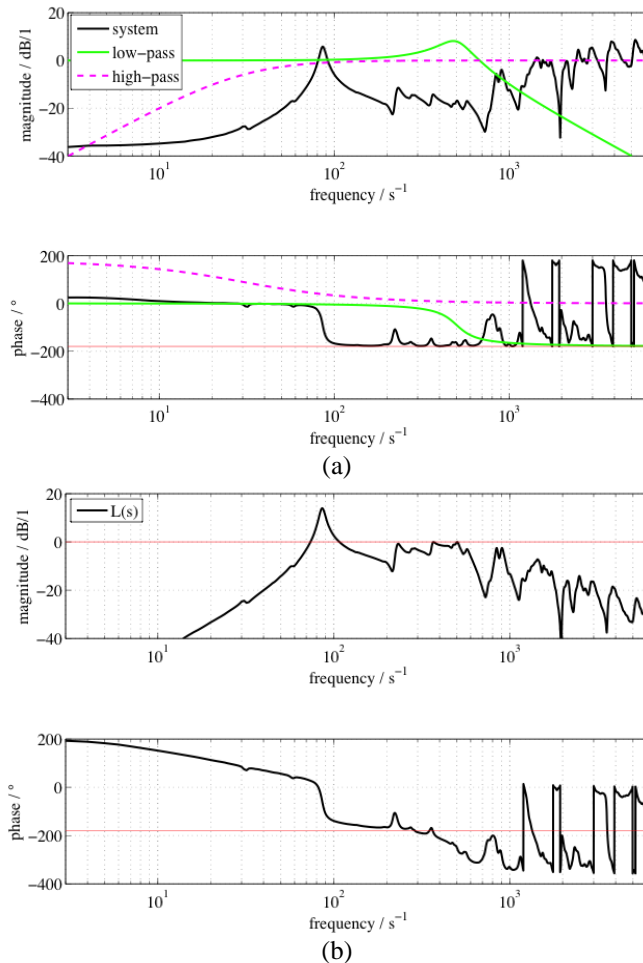


Fig. 17 Controller design for (11) - mode (Berger 2011)

The controller is designed in the frequency domain individually for each mode, see Fig. 16. Every closed loop consists of the following components: The system itself  $G_{ij}(s)$ , the controller  $R_{ij}(s)$  and the disturbance  $d(t)$  with the disturbance transfer function  $G_{ij,d}(s)$ . Therefore the modal controller error follows to

$$e_{ij}(t) = r_{ij}(t) - y_{ij}(t) = -y_{ij}(t) \tag{33}$$

for a vanishing command variable  $r_{ij}(t)$ . The overall aim to minimize the transfer function of the

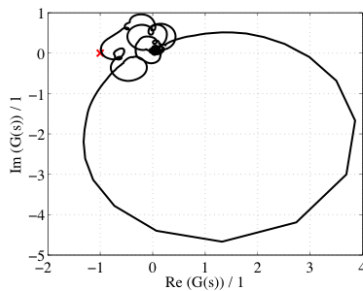
disturbance  $T_{y_{ij}/d}$  with

$$T_{y_{ij}/d} = \frac{G_{ij,d}}{1 + R_{ij}(s)G_{ij}(s)} \tag{34}$$

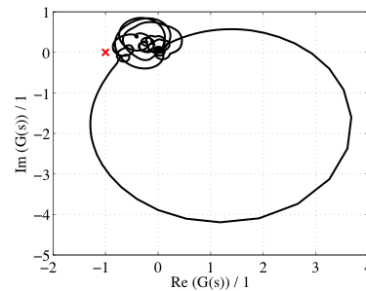
can be satisfied by maximizing the transfer function of the open loop  $L_{ij}(s) = R_{ij}(s)G_{ij}(s)$ . Thereby the conditions of a high magnitude over the controlled bandwidth for a high disturbance rejection, a small magnitude for higher frequencies for avoiding the amplifying of higher modes and criteria of relative stability in order to provide a stable feedback system must be fulfilled, see Nader (2008) or for further details Dorf and Bishop (2005).

Regarding exemplarily the transfer function for the first modal system shown in Fig. 17(a), a second order low-pass filter ( $LP_2(s)$ ), an additional second order high-pass filter ( $HP_2(s)$ ) and the proper selection of a proportional part  $K_p$  fulfill these requirements and yield to the open loop of the controlled system shown in Fig. 17(b) with the resulting function of the controller

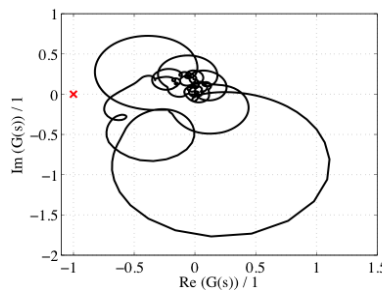
$$R_{ij}(s) = K_p LP_2(s)HP_2(s). \tag{35}$$



(a) Nyquist plot of the open loop of the first mode



(b) Nyquist plot of the open loop of the second mode



(c) Nyquist plot of the open loop of the third mode

Fig. 18 Nyquist plots of the implemented modal controllers

In order to verify the stability of the closed-loop system including the designed feedback control system with the applied modal controller the Nyquist stability criterion is used; in particular, the simplified Nyquist criterion can be used in our case, see (Lunze (1996)). Therefore, the Nyquist plot of the open loop system of all three modes to be controlled is shown in Fig. 18. All three plots prove an asymptotic stable behaviour of the closed loop system, as the point (-1,0)

in the phase plane is not encircled for  $\omega = 0 \dots \infty$ .

**Experimental results** As before the lateral velocities at  $x = 122$  mm and  $y = 175$  mm due to a loudspeaker excitation are measured; the result for a sine sweep excitation is shown in Fig. 19 together with the corresponding results for shunt damping. Note that the maximum voltages applied to the piezoelectric actuator array were constrained to  $\pm 100$  V.

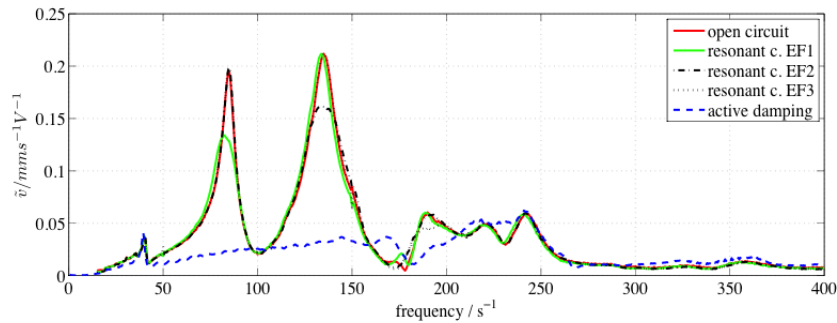


Fig. 19 Comparison of active and passive damping methods (sine sweep excitation)

For the first, second and third eigenfrequency the vibration amplitude was reduced by -18dB, -18dB and -7dB, a result that is clearly superior to the one for the passive shunt damping. Due to the fact that there are no more peaks in the controlled response, we cannot extract corresponding damping ratios for the case of active modal control. Finally, Fig. 20 presents the FFT-analysis of the uncontrolled and the actively controlled plate structure, when all three modes are actuated simultaneously. The input voltage of the loudspeaker was chosen as the superposition of three sinusoidal signals with the first three eigenfrequencies of the system as the three excitation frequencies; the amplitude ratios of the excitation were chosen such that the corresponding three tones were subjectively sensed with the same loudness. Thereby the amplitudes were reduced by -17dB, -13dB and -12dB. This effective active control in combination with the design of the modal transducer arrays led consequently to the patent Gerstmayr *et al.* (2011).

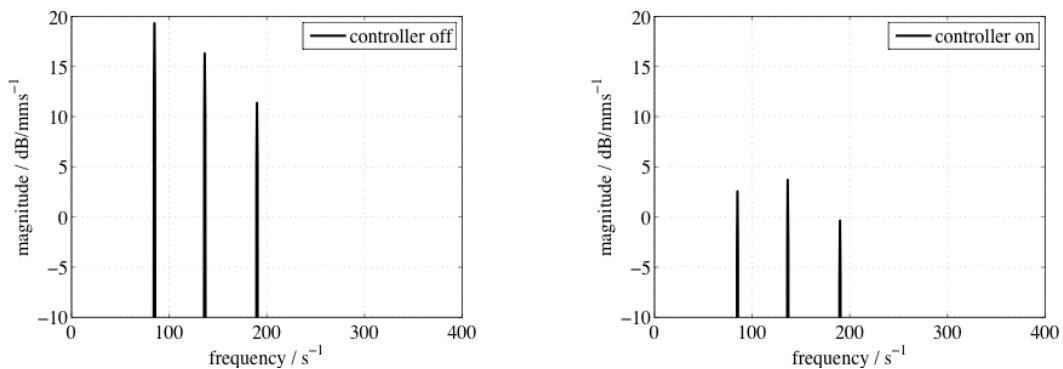


Fig. 20 FFT analysis of the first three eigenfrequencies (simultaneous excitation) (Berger 2011)

## 6. Conclusions

In this paper an active modal control technique and passive resonant shunt circuits for the suppression of vibrations of a rectangular plate with the help of distributed piezoelectric modal transducers have been evaluated and compared. Based on the Kirchhoff plate equations, a set of modal sensors/actuators has been found by adding nilpotent sensors/actuators, such that the interior of the plate domain can be left uncovered. This new distribution is especially attractive for damping transparent plates. The modal sensors/actuators were then implemented by applying distributed discrete piezoelectric transducers along the edge of an experimental setup. Their advantage to randomly placed sensors/actuators is to sense or actuate only the specific mode for which they are configured. After verifying both, the analytical and the discrete approach, the damping strategies have been implemented.

The modal control approach is suitable to result into a broad banded and very effective damping device. It can also handle variable stimulations at small expenses of efficiency. In this paper the first three eigenmodes could be suppressed with a reduction of up to -20dB, which is superior to other results reported in the literature. Shunt damping mechanisms are most suitable for an autonomous and light weighted system. Without the use of any active parts like power amplifiers, a shunt circuit with an inductance leads to an annihilation of the vibration at a certain frequency. Nonetheless, utilizing a resonant circuit with an additional resistor to avoid the appearing side peaks can still damp the vibration amplitude up to -5dB. The common challenge of high values for the inductance could be prevented by using the modal transducers due to higher piezoelectric capacitance without losing any damping efficiency. For handling more modes multi-mode techniques can be used.

## Acknowledgments

Support of the present work in the framework of the Comet-K2 Austrian Center of Competence in Mechatronics (ACCM) is gratefully acknowledged by the authors.

## References

- Alkhatib, R. and Golnaraghi, M.F. (2003), "Active structural vibration control: a review", *Shock Vib.*, **35**(5), 367-383.
- Berger, W. (2011), *Aktive Schwingungstilgung von Platten mit elektromagnetischen und piezoelektrischen Aktoren und Sensoren*, Diploma-Theses, Linz, Johannes Kepler University.
- Bonet, J. and Wood, R.D. (2008), *Nonlinear continuum mechanics for finite element analysis* 2nd Ed., Cambridge, University Press.
- Bruant, I. and Proslie, L. (2005), "Optimal location of actuators and sensors in active vibration control", *J. Intel. Mat. Syst. Str.*, **16**, 197-206.
- Crawley, E.F. (1994), "Intelligent Structures for Aerospace: A Technology Overview and Assessment", *AIAA J.*, **32**(8), 1689-1699.
- Den Hartog, J.P. (1985), *Mechanical vibrations*, New York, Dover Publications.
- Deraemaeker, A. and Preumont, A. (2006), "Vibration based damage detection using large array sensors and spatial filters", *Mech. Syst. Signal Pr.*, **20**, 1615-1630.

- Donoso, A. and Bellido, J.C. (2009), "Systematic design of distributed piezoelectric modal sensors/actuators for rectangular plates by optimizing the polarization profile", *Struct. Multidiscip. O.*, **38**(4), 347-356.
- Dorf, R. and Bishop, R. (2005), *Modern control systems* 10th Ed., New York, PEARSON Prentice Hall.
- Fuller, C.R., Elliot, S.J. and Nelson, P. A. (1996), *Active control of vibrations*, San Diego, Academic Press.
- Gabbert, U. and Tzou, H.S. (2000), "Preface", *Proceedings of the IUTAM-Symposium on Smart Structures and Structronic Systems*, (Eds. U. Gabbert and H.S. Tzou ), Kluwer Dordrecht, September.
- Gattringer, H., Nader, M., Krommer, M. and Irschik, H. (2003), "Collocative PD control of circular plates with shaped piezoelectric actuators/sensors", *J. Vib. Control*, **9**, 965-982.
- Gerstmayr, J., Nader, M. and Berger, W. (2011), *Vorrichtung und Verfahren zur Reduktion einer Schwingung einer insbesondere transparenten Platte*, Austria Patent AT4752011.
- Gupta, V., Sharma, M. and Thakur, N. (2010), "Optimization criteria for optimal placement of piezoelectric sensors and actuators on a smart structure: a technical review", *J. Intel. Mat. Syst. Str.*, **21**, 1227-1243.
- Hac, A. and Liu, L. (1993), "Sensor and actuator location in motion control of flexible structures", *J. Sound Vib.*, **167**, 239-261.
- Hagood, N.W. and Flotow, A. (1991), "Damping of structural vibrations with piezoelectric materials and passive electrical networks", *J. Sound Vib.*, **146**( 2), 243-268.
- Hansen, C. and Snyder, S. (1997), *Active control of noise and vibration*, London, E & FN Spon.
- Herold, S. (2003), *Simulation des dynamischen und akustischen Verhaltens aktiver Systeme im Zeitbereich*, Phd Theses, Darmstadt: University of Darmstadt.
- Hwang, J.K., Choi, C.H., Song, C.K. and Lee, J.M. (1997), "Robust LQG control of an all-clamped thin plate with piezoelectric actuators/sensors", *IEEE/ASME T. Mech.*, **2**( 3), 205-212.
- Inman, D. (1997), "Active modal control for smart structures", *Philos. T. R. Soc. A*, **359**(1778), 205-219.
- Irschik, H. and Ziegler, F. (1988), "Dynamics of linear elastic structures with selfstress: a unified treatment for linear and nonlinear problems", *Zeitschrift für Angewandte Mathematik und Mechanik*, **68**, 199-205.
- Irschik, H., Krommer, M., Belyaev, A.K. and Schlacher, K. (1998), "Shaping of piezoelectric sensors/actuators for vibrations of slender beams: coupled theory and inappropriate shape functions", *J. Intel. Mat. Syst. Str.*, **9**, 546-554.
- Irschik, H., Krommer, M. and Pichler, U. (1999), "Shaping of distributed piezoelectric sensors for flexural vibrations of smart beams", *Proceedings of the SPIE's 6th Annual International Symposium on Smart Structures and Materials*, (Ed.V.V. Varadan), Mathematics and Control in Smart Structures , March .
- Irschik, H. (2002), "A review on static and dynamic shape control of structures by piezoelectric actuation", *Eng. Struct.*, **24**, 5-11.
- Irschik, H., Krommer, M. and Pichler, U. (2003), "Dynamic shape control of beam - type structures by piezoelectric actuation and sensing", *Int. J. Appl. Electrom.*, **17** (1-3), 251-258.
- Kirchhoff, G. (1850), "Über das Gleichgewicht und die Bewegung einer elastischen Scheibe", *Zeitschrift für Reine und Angewandte Mathematik*, **40**, 51-58.
- Krommer, M. (2003), "The significance of non-local constitutive relations for composite thin plates including piezoelectric layers with prescribed electric charge", *Smart Mater. Struct.*, **12**, 318-330.
- Krommer, M. and Varadan, V. (2005), "Control of bending vibrations within subdomains of thin plates - part I: theory and exact solution", *J. Appl. Mech. - T ASME*, **72** (3), 432-444.
- Krommer, M. and Irschik, H. (2007), "Sensor and actuator design for displacement control of continuous systems", *Smart Struct. Syst.*, **3**(2), 147-172.
- Krommer, M., Zellhofer, M. and Heilbrunner, K.H. (2009), "Strain-type sensor networks for structural monitoring of beam-type structures", *J. Intel. Mat. Syst. Str.*, **20**, 1875-1888.
- Kugi, A. (2001), *Non - linear control based on physical models*, London, Springer.
- Lee, C.K. and Moon, F.C. (1990), "Modal sensors/actuators", *J. Appl. Mech. - T ASME*, **57**, 434-441.
- Liu, S.C., Tomizuka, M. and Ulsoy, G. (2005), "Challenges and opportunities in the engineering of intelligent structures", *Smart Struct. Syst.*, **1**(1), 1-12.
- Lunze, J. (1996), *Regelungstechnik I, Systemtheoretische Grundlagen Analyse und Entwurf einschleifiger Regelungen*, Berlin, Springer.
- Lurie, A.I. (2002), *Analytical mechanics*, Berlin Heidelberg New York, Springer.

- Ma, K. (2003), "Adaptive non-linear control of a clamped rectangular plate with PZT patches", *J. Sound Vib.*, **264**, 835-850.
- Moheimani, S.O.R. and Fleming, A. (2006), *Piezoelectric transducers of vibration control and damping*, London, Springer.
- Mura, T. (1987), *Micromechanics of defects in solids* 2nd Ed., Springer.
- Nader, M., Gattringer, H., Krommer, M. and Irschik, H. (2003), "Shape control of flexural vibrations of circular plates by shaped piezoelectric actuation", *J. Vib. Acoust.*, **125**( 1), 88-94.
- Nader, M. (2008), *Compensation of vibrations in smart structures: shape control*, experimental realization and feedback control, Linz, Trauner.
- Nemenyi, P. (1931), "Eigenspannungen und Eigenspannungsquellen", *Zeitschrift für Angewandte Mathematik und Mechanik*, **11**, 1-8.
- Nestorović, T., Lefévre, J. and Gabbert, U. (2007), "Model-based active noise control of a piezoelectric structure", *J. Mech.*, **26**(2), 71-77.
- Niederberger, D. (2005), *Smart damping materials using shunt control* , PhD. Thesis, Zurich, ETH Zurich.
- Nyashin, Y., Lokhov, V. and Ziegler, F. (2005), "Decomposition method in linear elastic problems with eigenstrain", *Zeitschrift für Angewandte Mathematik und Mechanik (ZAMM)*, **85**(8), 557-570.
- Preumont, A. (2002), *Vibration control of active structures* 2nd Ed., New York, Springer.
- Preumont, A., Francois, A., De Man, P. and Piefort, V. (2003), "Spatial filters in structural control", *J. Sound Vib.*, **265**, 61-79.
- Preumont, A., Francois, A., De Man, P., Loix, N. and Henriouille, K. (2005), "Distributed sensors with piezoelectric films in design of spatial filters for structural control", *J. Sound Vib.*, **282**, 701-712.
- Reissner, H. (1931), "Selbstspannungen elastischer Gebilde", *Zeitschrift für Angewandte Mathematik und Mechanik*, **11**, 59-70.
- Schöftner, J. and Irschik, H. (2009), "Passive damping and exact annihilation of vibrations of beams using shaped piezoelectric layers and tuned inductive networks", *Smart Mater. Struct.*, **18**(12), 1250081-1250089.
- Schöftner, J. and Krommer, M. (2012), "Single point vibration control for a passive piezoelectric Bernoulli-Euler beam subjected to spatially varying harmonic loads", *Acta Mech.*, **223**(8), 1983-1998.
- Selvadurai, A.P.S. (2000), *Partial differential equations in mechanics* 2, Berlin Heidelberg, Springer.
- Tani, J., Takagi, T. and Qiu, J. (1998), "Intelligent material systems: application of functional materials", *Appl. Mech. Rev.*, **51**, 505-521.
- Trindade, M.A. and Benjeddou, A. (2009), "Effective electromechanical coupling coefficients of piezoelectric adaptive structures: critical evaluation and optimization", *Mech. Adv. Mater. Str.*, **16**( 3), 210-223.
- Tzou, H.S., Zhong, J.P. and Hollkamp, J.J. (1994), "Spatially distributed orthogonal piezoelectric shell actuators: theory and applications", *J. Sound Vib.*, **177**( 3), 363-378.
- Yu, Y., Zhang, X.N. and Xie, S.L. (2009), "Optimal shape control of a beam using piezoelectric actuators with low control voltage", *Smart Mater. Struct.*, **18**( 9), 095005.
- Zehetner, Ch. and Irschik, H. (2005), "Displacement compensation of beam vibrations caused by rigid-body motions", *Smart Mater. Struct.*, **14**, 862-868.
- Zenz, G. (2011), *Shunt damping - Elektrische Netzwerke zur Schwingungsdämpfung mit piezoelektrischen Sensoren/Aktoren*, Linz, Trauner.